Electronic Journal of Biotechnology 65 (2023) 45–55

Contents lists available at ScienceDirect

Electronic Journal of Biotechnology

journal homepage: www.elsevier.com/locate/ejbt

Research Article

A novel nanocomposite based on mycosynthesized bimetallic zinc-copperoxide nanoparticles, nanocellulose and chitosan: Characterization, antimicrobial and photocatalytic activities

Mohamed S. Hasanin [a,*], Amr H. Hashem [b,*], Abdulaziz A. Al-Askar [c], Józef Haponiuk [d], Ebrahim Saied [b]

[a] Cellulose & Paper Department, National Research Centre, El-Buhouth St., Dokki 12622, Egypt
[b] Botany and Microbiology Department, Faculty of Science, Al-Azhar University, Cairo 11884, Egypt
[c] Department of Botany and Microbiology, Faculty of Science, King Saud University, P.O. Box 2455, Riyadh 11451, Saudi Arabia
[d] Department of Polymer Technology, Faculty of Chemistry, Gdańsk University of Technology, G. Narutowicza 11/12 80-233, Gdańsk, Poland

GRAPHICAL ABSTRACT

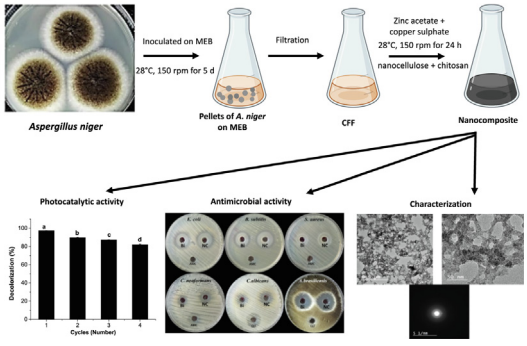

ARTICLE INFO

Article history:
Received 4 April 2023
Accepted 17 May 2023
Available online 10 July 2023

Keywords:
Antimicrobial activity
Bimetallic zinc-copper oxides nanoparticles
Candida albicans
Chitosan
Cryptococcus neoformans
Mycosynthesis
Nanocellulose
Nanocomposite
Nanomaterials
Photocatalytic activity

ABSTRACT

Background: Recently, nanomaterials have received much attention due to their important role in solving medical and environmental problems. In the present study, a novel nanocomposite based on mycosynthesized bimetallic zinc-copper oxides nanoparticles, nanocellulose, and chitosan was ready through an ecofriendly method. Characterization, antimicrobial and photocatalytic activities were evaluated.

Results: The result revealed that the prepared nanocomposite exhibited antibacterial activity against *Bacillus subtilis*, *Escherichia coli* and *Staphylococcus aureus*, where MICs were 7.81, 31.25 and 62.5 μg mL^{-1}. As well, the nanocomposite showed potential antifungal activity against *Aspergillus brasiliensis* where MIC was 7.81 μg mL^{-1}, but had minimal antifungal efficacy against *Cryptococcus neoformans* and *Candida albicans* where the MIC was 250 μg mL^{-1} for each other. Furthermore, the nanocomposite had photocatalytic activity. The bimetallic and nanocomposite materials were characterized via physiochemical and topographic analysis.

Conclusions: In conclusion, the prepared nanocomposite based on mycosynthesized bimetallic zinc-copper oxides nanoparticles nanocellulose and chitosan has antimicrobial and photocatalytic activities which can be applied to various environments.

Peer review under responsibility of Pontificia Universidad Católica de Valparaíso.
* Corresponding authors.
E-mail addresses: sido_sci@yahoo.com (M.S. Hasanin), amr.hosny86@azhar.edu.eg (A.H. Hashem).

https://doi.org/10.1016/j.ejbt.2023.05.001

How to cite: Hasanin MS, Hashem AH, Al-Askar AA, et al. A novel nanocomposite based on mycosynthesized bimetallic zinc-copper oxides nanoparticles, nanocellulose and chitosan: Characterization, antimicrobial and photocatalytic activities. Electron J Biotechnol 2023;65. https://doi.org/10.1016/j.ejbt.2023.05.001.

1. Introduction

Textile dyeing mill effluent contains many kinds of dye in an extremely concentrated dye discharge. The majority of dyestuffs have complex aromatic compounds that are difficult to degrade naturally [1]. Textile dyeing companies typically employ the azo dye RR 195. This dye has a reactive group that is usually a heterocyclic aromatic ring replaced with chloride and fluoride [2]. The reactive azo dyes, in particular, are worth mentioning from this perspective. Among synthetic dyes, azo dyes are extremely widely employed on a commercial scale, accounting for more than 70% of colors used in industries such as textiles. Some physical, chemical, and biological techniques for dye removal include chemical oxidation, flocculation, photochemical degradation, membrane filtration, and aerobic and anaerobic biological degradation. None of these technologies are without limitations, and none of them are capable of totally removing dyes from wastewater [3]. Nanotechnology is being employed in a variety of fields right now, involving wastewater treatment and the environment, due to its small size, specific surface area, and high surface reactivity [4]. A range of physical and chemical processes, including hydrothermal microwave irradiation, thermal decomposition, sol-gel, sonochemical, fast precipitation, and colloidal thermal synthesis for the synthesis of desired shapes and characteristics of nanomaterials have been presented [5]. However, these techniques call for a lot of effort, a lot of energy, a lot of complex routes, and a lot of expensive and dangerous substances [6]. Therefore, creating new biocompatible methods that may assist in overcoming the above restrictions is of utmost importance in the synthesis of nanomaterials [7]. Records indicate that the physical and chemical methods of making metal and metal oxide nanoparticles are progressively being replaced by biological techniques called biosynthesis or "green" nanoparticle production [8]. The biological process of production of metal or metal oxide nanoparticles involves using plant, algal, bacterial, yeast, fungal and other microbial extracts as reducing agents for the synthesis of nanoparticles which are biocompatible and can be produced in large amounts [9,10]. CuONPs are strongly interacting nanomaterials with a wide range of biological features, including antioxidant capacity, antifungal and antibacterial activity, cytotoxic efficiency and drug delivery against cancerous and tumor cells. Among other biological organisms, bacteria, fungi, actinomycetes, algae, and plants all generate CuONPs either extracellularly or intracellularly [11]. Many investigators have documented many techniques for producing CuONPs, including sonochemical synthesis, template methods using surfactants, biosynthesis techniques, hydrothermal ultrasound irradiation, electron beam lithography, decomposition of copper acetate, sol–gel, microwave-assisted protocols, and solid-state reactions [12,13,14,15]. Additionally, it has been shown that the way CuONPs are made has an effect on both their physical traits and poisonous behavior [6]. Fungi are the preferred microorganisms because of their fast growth, bio-properties, and simple structures that are easy to operate. Furthermore, these organisms create the most biomolecules, which induce the synthesis of NPs. Fungi may very well be able to synthesize a range of NPs via intracellular and extracellular pathways, and many investigations have been carried out on the creation of metallic and oxide NPs such as zinc, gold, titanium, copper and silver [16,17,18]. The capacity of many fungal species to release large quantities of proteins or enzymes and the ease with which they may be traded in laboratories account for their extensive usage [19]. In addition, due to their tolerance and capacity to bioaccumulate metals, fungi have received increased interest since they are involved in the study of the biological production of metallic nanomaterials [20]. Furthermore, many fungal species have extremely quick growth rates and large numbers of mass cells, rendering it quite straightforward to keep them in a certain laboratory [21]. The most widely used methods for removing colors from industrial wastewater include coagulation and flocculation, advanced oxidation technology, photodegradation, membrane separation and biological treatments. These methods have drawbacks for instance i) insufficient removal of dyes leading to polluted influents, [22] high operating costs because of energy needs, and ii) the production of toxic products like sludge and new dangerous chemical compounds [23,24]. Utilizing biosorbents, which are biodegradable and made from agro-industrial wastes, is a more modern method [25,26]. Chitosan is a biopolymer composed of 2-amino-2-deoxy-D-glucopyranose units [27]. CS is the second most widespread polymer in nature, manufactured mostly by marine organisms such as shrimp and crabs [28]. Non-toxicity, biodegradability, antibacterial activity, and biocompatibility are only a few of the significant and diverse features of CS. There has been a tremendous surge in interest in recent years in ZnO/Chitosan nanocomposite due to its novel uses, including UV protection and antibacterial properties [29]. This study's originality comes from the fact that the synthesized nanocomposite (ZnO-CuO NPs/CSC) acted as an inhibitor for most organisms at low concentrations. Moreover, the photocatalytic activity was investigated and observed. There has not been much research done on this system in the literature. The goal of this study was to synthesize a nanocomposite based on bimetallic zinc-copper oxides nanoparticles and chitosan using an ecofriendly method, and also to evaluate its antibacterial, and antifungal activities as well as the photocatalytic degradation of azo dye RR-195.

2. Experimentation techniques

2.1. Materials

In this research, copper sulfate pentahydrate, zinc acetate pentahydrate, Reactive Red 195 (RR195), hydrochloric acid, sodium hydroxide and acetic acid were acquired from Sigma Aldrich, Cairo, Egypt. Chitosan for this research was bought from Sigma Aldrich (St. Louis, viscosity 275.9 cps, molecular weight 650,000 and degree of deacetylation 85.5%). The nanocellulose applied to this work was produced and described in our earlier work. We bought the Malt Extract Agar (MEA) and Malt Extract Broth (MEB) media from Merck in Germany.

2.2. Fungal growth conditions

In earlier times, *Aspergillus niger AH1* was isolated in our work from a soil sample and was noted in the Gene Bank with accession

number MW680847.1. *A. niger* was cultured on MEA at 28°C ± 2°C for 5 d, and then preserved in the refrigerator at 4°C until use.

2.3. Biosynthesis of bimetallic ZnO-CuO NPs utilizing the biomass filtrate from A. niger AH1

Three discs of the fungal strain *A. niger* AH1 (7 mm in diameter) were inoculated on MEB broth medium and incubated for 5 d at 28°C ± 2°C, pH adjusted to 6.0, and shaking conditions (150 rpm). Following the incubation period, the collected biomass (15g) was rinsed with deionized and sterilized H_2O, then resuspended in 100 mL of distilled water at 28°C ± 2°C, 150 rpm for 3d. Filtration was carried out to obtain the fungal biomass filtrate, which was then used to make ZnO-CuO NPs as follows: 2.0 mM of zinc acetate pentahydrate and 4.0 mM of $CuSO_4 \bullet 5H_2O$ were added to 100 mL of fungal biomass filtrate for 24 h at 28°C ± 2°C, 150 rpm, pH 9 in the dark. A dark green color appeared in the filtrate, which was then oven-dried at 120°C for 24 h [30].

2.4. Preparation of nanocomposite

Nanocomposite was prepared using CS solution 1% (wt/v) dissolved in 1% (wt/v) acetic acid solution. The CS solution was stirred for 1 h at 70°C after adding 0.1 gm nanocellulose developed in accordance with our earlier work. The prepared nanocomposite was ultrasonicated for 5 min using an ultrasonic prop. For usage and further research, the obtained material was lyophilized and stored in the refrigerator.

2.5. Characterization of nanocomposite (ZnO-CuO NPs/CSC)

Characterizations of the materials were carried out using physiochemical identifications including ultraviolet visible spectroscopy (UV–Vis) and the spectra were measured using V-630 UV–vis spectrophotometer (Jasco, Japan) in the range of 1000–200 nm. Fourier-transform infrared spectroscopy (FTIR) was analyzed using "Spectrum Two IR Spectrometer – PerkinElmer, Inc., Shelton, USA". Different X-ray diffraction patterns (XRD) were investigated using a Diano X-ray diffractometer (Philips). The morphological study included a scanning electron microscope (SEM) (SEM, Quanta FEG 250, FEI, Republic of Czech) attached to an EDX Unit (Energy Dispersive X-ray Analyses) for EDX. High-resolution transmission electron microscope (HRTEM) JEOL–JEM-1011, Japan.

2.6. Antimicrobial activity

Antimicrobial activity of ZnO-CuO NPs and ZnO-CuO NPs/CSC was assessed against *Staphylococcus aureus* ATCC 2592, *Bacillus subtilis* ATCC 6051, *Escherichia coli* ATCC 25922, *Candida albicans* ATCC 90028, *Cryptococcus neoformans* ATCC 14116, *Aspergillus brasiliensis* ATCC 16404. The diffusion test in agar was performed in accordance with Standards [31,32] with slight modifications. The selected bacterial/fungal strains were grown on nutrient agar/PDA media for 24 h at 37°C/72 h at 30°C, respectively. In wells of bacterial/fungal seeded medium, 100 µl of ZnO-CuO NPs and ZnO-CuO NPs/CSC, standard antibiotic/antifungal (Amoxicillin/clavulanate)/Clotrimazole (CLT), at concentration 1000 µg mL^{-1} were added, and plates were chilled for 2 h before incubation at 37°C for 24 h. After 72 h of incubation at 30°C, the inhibition zone diameter was determined on all PDA plates. ZnO-CuO NPs and ZnO-CuO NPs/CSC, AMC, and CLT agents were prepared in concentrations ranging from 1000 to 3.9 µg mL^{-1} to determine the minimal inhibitory concentration.

2.7. Photocatalytic activity of Reactive Red 195 (RR195) dye solution agents

The capability of photocatalysis for ZnO-CuO NPs/CSC was determined by observing the degradation of RR195 dye at various dye concentrations (25, 50, 75, 100, 150 and 200 mg mL^{-1}) by using 100 µg mL^{-1} of nanocomposite ZnO-CuO NPs/CSC under sunlight conditions. The photocatalytic experiment involved mixing 100 mL of various RR195 dye solutions in triplicate with various concentrations of ZnO-CuO NPs/CSC and incubating the mixture at room temperature with shaking for 3 h. The effectiveness of decolorization was determined, where each treatment was centrifuged at 10000 rpm for 3.0 min. and measured at (λ_{max}) 538 nm [33] of the Reactive Red 195 dye solution by using UV–Vis spectroscopy (JENWAY 6305 Spectrophotometer). The decolorization percentage (%) of RR195 dye was measured using Equation 1 [34].

$$D\,\% = \frac{\text{dye (i)} - \text{dye (1)}}{\text{dye (i)}} \text{ X } 100 \quad (1)$$

D (%) = is the percentage of decolorization.
Dye (i) = the initial absorbance.
Dye (1) = the final absorbance.

For the fourth cycle, the nanocomposite ZnO-CuO NPs/CSC reusability in the degradation of RR195 was accomplished under ideal circumstances. Before being employed in the second cycle, the catalyst from the first cycle was recovered by centrifugation, exposed to two washings with distilled water, and oven-dried at 80°C to reduce water content.

2.8. Effect of environmental conditions on decolorization of Reactive Red 195 (RR195)

Different parameters were taken, such as different incubation times, different incubation temperatures, nanocomposite concentrations, and different pH values, to increase the decolorization of RR195. The experiment was conducted in three replicates, and the results have been monitored using the UV–Visible spectrophotometer. The experiments were designed at different incubation times (30, 60, 90, 120, 150, 180, 240 and 300 min) to select the best incubation time for decolorization of RR195; incubation temperatures of 25, 30, 32 and 40°C; different concentrations of nanocomposite (1.0, 2.0, 3.0, 4.0 and 5.0 µg mL^{-1}) and different pH values (5, 6, 7, 8 and, 9) on dye decolorization were tested at a constant dye concentration of 25 ppm. At the end of each incubation period, the dye decolorization (%) was assayed at 538 nm by using UV–Vis spectroscopy (JENWAY 6305 Spectrophotometer).

2.9. Statistical analysis

All of the results shown are the averages of three different replicates. SPSS v18 was used to analyze the data. A t-test or an ANOVA was used to analyze the mean difference between the treatments, and then, a Tukey HSD test was performed At P 0.05.

3. Results and Discussion

3.1. Synthesis and characterization of the nanocomposite

The strain *Aspergillus* sp. was able to synthesize various NPs [35]. The potential to biosynthesize nanocomposite ZnO-CuO NPs/CSC was demonstrated in this work by the metabolites of the fungus *A. niger* AH1 which enhanced the production process, decreased the aggregation, and produced a smaller size [36]. Indeed, factors that affected the formulation of nanoparticles using

fungal media and based on the function groups of the metabolites in media act as capping agents that affect also the productivity recorded in our work to about 52% based on weight [37,38,39]. CuONPs were created by Mani et al. [17] from the extracellular extract of the fungus *A. terreus*. Ghareib et al. [40] synthesized the CuONPs by using the biomass of *A. fimigatus*. In contrast, Streptomyces MHM38 was used by Bukhari et al. [41] to biosynthesize copper oxide nanoparticles. Kumar et al. [42] reported that zinc oxide nanoparticles were biofabricated by Dictyota dichotoma endophytic fungi. Otherwise, some articles dealt with the biosynthesis of ZnONPs via different biological extractions, such as plant extract or microbiological medium [43,44]. On the other hand, Fouda et al. [45] used maghemite nanoparticles (γ-Fe2O3-NPs) produced by *Penicillium expansum* [46] for wastewater treatment. Also, Albalawi et al. [47] have synthesized silica nanoparticles by using *A. niger*. Saied et al. [35] biosynthesized magnesium oxide nanoparticles (MgO-NPs) by using *A. terreus.* Additionally, ZnO-CuO-NPs were previously preprepared [48,49]. Fouda et al. [50] is used in treatment via photocatalytic. In fact, the bimetallic nanoparticle is effective in several applications, especially wastewater treatment. Moreover, the loading of nanoparticles into nanocomposite increases and improves the efficiency and stability, which are crucial for the usage of the material.

3.2. Characterization

The characterizations of ZnO-CuO NPs and ZnO-CuO NPs/CSC were carried out using a physiochemical analysis as well as topographical examinations. Fig. 1A shows UV–visible spectra of ZnO-CuO NPs and ZnO-CuO NPs/CSC. ZnO-CuO NP spectrum observed peaks at 326, 365 and 410 nm that are referred to as heterojunction effectively of metal oxides and affirmed the mycosynthesis of ZnO-CuO NPs with a nice agreement with previous publications [49,51,52]. On the other hand, the ZnO-CuO NPs/CSC spectrum was observed with a strong small band at 275 nm and broadband at 395 nm that recorded a shift in the the original peak positions that are referred to as a strong combination between metals and nanocomposite components [53,54].

FTIR was shown in Fig. 1B and illustrated the raw fungal medium, ZnO-CuO NPs and ZnO-CuO NPs/CSC as well as the neat components. The spectra of fungal medium filtrate bands at 3263, 2940, 2861, 1719, 1577, 1386, and 1031 cm^{-1} that referred to hydroxyl groups vibration stretching, C–H groups asymmetric stretching vibration of aliphatic groups, polyphenol skeleton of aromatic structures, C-O carbohydrate bond, respectively [55,56,57]. In the country, FTIR analysis is used to elucidate the functional groups involved in the reduction/capping the silver ions to the nano-scale. Additionally, ZnO-CuO NPs spectrum illustrated significant changes in comparison with the blank fungal medium, whereas the OH group stretching vibration band intensity in nanoparticle spectrum was eliminated as well as CH stretching vibration band and carbohydrate bands were shifted to the lower frequency. Moreover, two characteristic bands were assigned at 700 and 460 cm^{-1} and are referred to as CuO and ZnO, respectively [49]. Otherwise, the nanocomposite components involved, NC and CS, were observed a typical spectra of polysaccharide with hydroxyl group band at around 3400 cm^{-1} that is overlapping with NH group band in the case of chitosan. Additionally, CH group stretching was assigned at around 2930 cm^{-1} for both polysaccharides, and the carbohydrate band was observed at around 1030 cm^{-1} as well. On contrary, ZnO-CuO NPs/CSC spectrum observed a high shift in Hydroxyl group to lower frequency as a result to the interaction of ZnO-CuO NPs with the polysaccharide structure included NH and OH. However, CH stretching vibration was overlapped with hydroxyl group as a result of interaction of hydroxyl groups of NC with NH of CS. In addition, the carbohydrate band was assigned as high-intensity band as resulted to the electron withdrawing toward bond as result attract of lone pairs of electrons on oxygen group of metal oxide. Additionally, the bands of metal oxide were assigned with slight shifting to the higher frequency.

Fig. 1C has illustrated the XRD patterns of ZnO-CuO NPs and ZnO-CuO NPs/CSC. Consequently, the ZnO-CuO NP pattern was observed in both ZnO and CuO patterns. For ZnO, peaks were presented at 2θ = 31.66°, 34.26°, 36.06°, 47.56°, 56.43°, 62.84° and match well with the PDF card (JCPDS No.36–1451) of the Wurtzite structure of ZnO [58]. Furthermore, for CuO, the diffraction peaks were recorded at 2θ = 36.06°, 38.76°, 59°, 62.7°, 67.5°, 68.8° and 73.5° and it confirms that the monoclinic phase of CuO is well matched with standard JCPDS (48–1548) [59,60]. In other words, the nanocomposite ZnO-CuO NPs/CSC pattern has assigned two humps of carbohydrate polymer at around 11° and 21° that reported the chitosan and nanocellulose [61]. Additionally, the ZnO and CuO peaks were observed with low intensity as well.

Topographical study included SEM and TEM, as well as EDX and SAED patterns were observed in Fig. 2. The SEM image in Fig. 2A has shown a bimetallic with metallic shiny particle aggregated with a size lowest than 50 nm. In addition, the nanocomposite (Fig. 2B) has observed ZnO-CuO NPs attached to the surface of nanocomposite matrix at low magnification. Additionally, the high magnification was performed in ZnO-CuO NPs coated and attached with ZnO-CuO NPs/CSC matrix and formed a rough surface that could be occupied in dye adsorption. Moreover, the EDX chart of ZnO-CuO NPs (Fig. 2C) has shown atoms that contain zinc, copper and oxygen. However, ZnO-CuO NPs/CSC (Fig. 2D) has clear presences of copper, zinc and oxygen atoms. Besides, the TEM images of nanocomposite with low and high magnifications (Fig. 2E and F) were performed by the intermolecular structure of ZnO-CuO NPs/CSC as a network of polysaccharide matrix doped with ZnO-CuO NPs. In addition, the SEAD (Fig. 2F) observed a polycrystalline nature of ZnO-CuO NPs/CSC that could relate to the intermolecular structure observed by TEM image.

3.3. Antimicrobial activity

The antimicrobial activity of the prepared bimetallic nanoparticles and nanocomposite was assessed as shown in Fig. 3 and Table 1. Results revealed that bimetallic nanoparticles and nanocomposite exhibited antimicrobial activity toward selected microbial strains [62]. Furthermore, the prepared nanocomposite exhibited antimicrobial activity higher than bimetallic nanoparticles as shown in Fig. 3. The prepared nanocomposite had antibacterial activity against *E. coli, B. subtilis and S. aureus* where inhibition zones were 23, 28 and 20 mm, respectively. As well, nanocomposite exhibited promising antifungal activity toward *C. albicns, C. neoformans* and *A. brasiliensis* where inhibition zones were 15, 17 and 28 mm. Furthermore, bimetallic nanoparticles gave antimicrobial activity against *E. coli, B. subtilis, S. aureus, C. albicns, C. neoformans* and *A. brasiliensis* where inhibition zones were 19, 23, 16, 11, 12 and 25 mm, respectively. On the other hand, AMC did not exhibit any activity on all tested bacterial strains, but CLT gave weak antifungal activity against all tested fungal strains. Furthermore, MICs of both bimetallic nanoparticles and nanocomposite against all tested strains were detected as illustrated in Table 1. Results revealed that MICs of nanocomposite were lower than MICs of bimetallic nanoparticles, and this indicates that nanocomposite has higher efficacy than bimetallic nanoparticles. MICs of nanocomposite against *E. coli, B. subtilis, S. aureus, C. albicns, C. neoformans* and *A. brasiliensis* were 31.25, 7.81, 62.5, 250, 250, 7.81 μg mL^{-1} respectively. Also, MICs of bimetallic nanoparticles against *E. coli, B. subtilis, S. aureus, C. albicns, C. neoformans* and *A. brasiliensis* were 125, 31.25, 125, 500, 1000 and 15.62 μg mL^{-1} respectively. Electrostatic interactions that cause ROS generation,

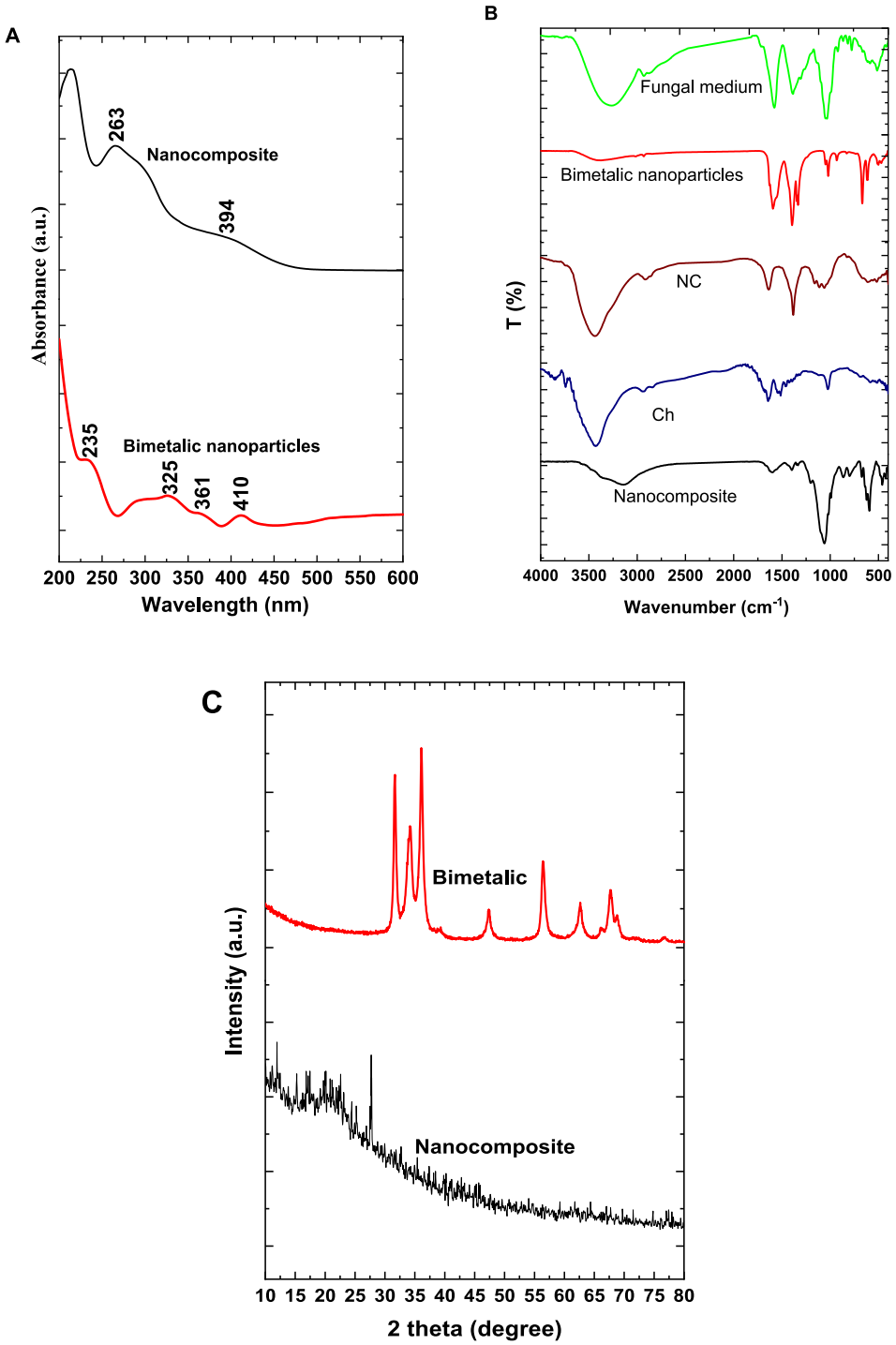

Fig. 1. UV–vis absorption spectra of ZnO-CuO NPs and ZnO-CuO NPs/CSC (A). FTIR of ZnO-CuO NPs and ZnO-CuO NPs/CSC as well as its parent materials (B). XRD pattern of ZnO-CuO NPs and ZnO-CuO NPs/CSC (C).

oxidative stress, cell membrane damage, disruption of proteins and enzymes, protein binding that disrupts homeostasis (electron transport chain disruption), signal transduction inhibition, and genotoxicity are possible mechanisms of action for ZnO-CuO NPs [63,64,65].

3.4. Photocatalytic activity of RR195 using ZnO-CuO NPs/CSC

The results in Fig. 4 illustrated that the decolorization percentages of RR195 dye by using nanocomposite ZnO-CuO NPs/CSC were 69.8 ± 0.51% and 24.5 ± 0.72% at 25, 150 mg mL^{-1} of RR195 dye concentration. Due to these results, when the dye concentration was increased, the decolorization percentage decreased. The high decolorization percentage occurred at 25 mg mL^{-1} of RR195 dye, and this concentration was selected to complete this study. Fig. 4's findings illustrate the impact of environmental factors on the decolorization of the RR195 dye, including incubation durations, temperatures, adsorbent concentrations, and pH values. The best incubation time for high decolorization of RR195 dye (80.5 ± 0.34%) occurred at 120 min. The increasing incubation time

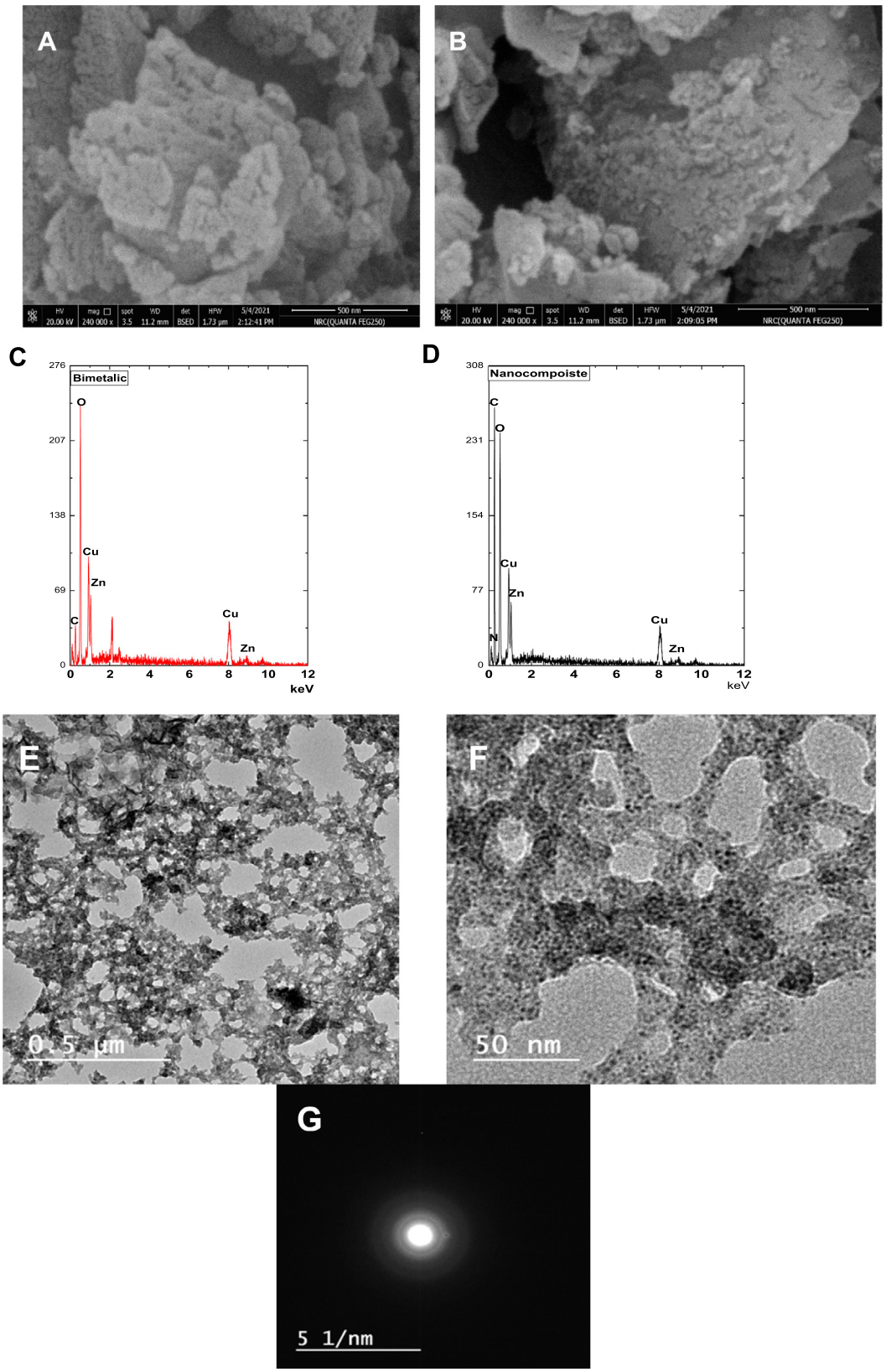

Fig. 2. Topographical study included SEM images of bimetallic (A), nanocomposites (B) and EDX chart of bimetallic (C) and nanocomposite (D). TEM of nanocomposites with low magnification (E), high magnification (F) and SAED pattern of nanocomposite (G).

led to the discharge of dye in the solution and a decrease in its decolorization. The decolorization percentage of RR195 dye was reached to 97% ± 0.57% at 32°C, pH 4.0 and 3 µg mL^{-1} of ZnO-CuO NPs/CSC after 120 min of incubation under sunlight conditions. According to Ali et al. [66], the degradation of the RR 195 dye over-produced zinc oxide was 91–94% after 70 min. The degree

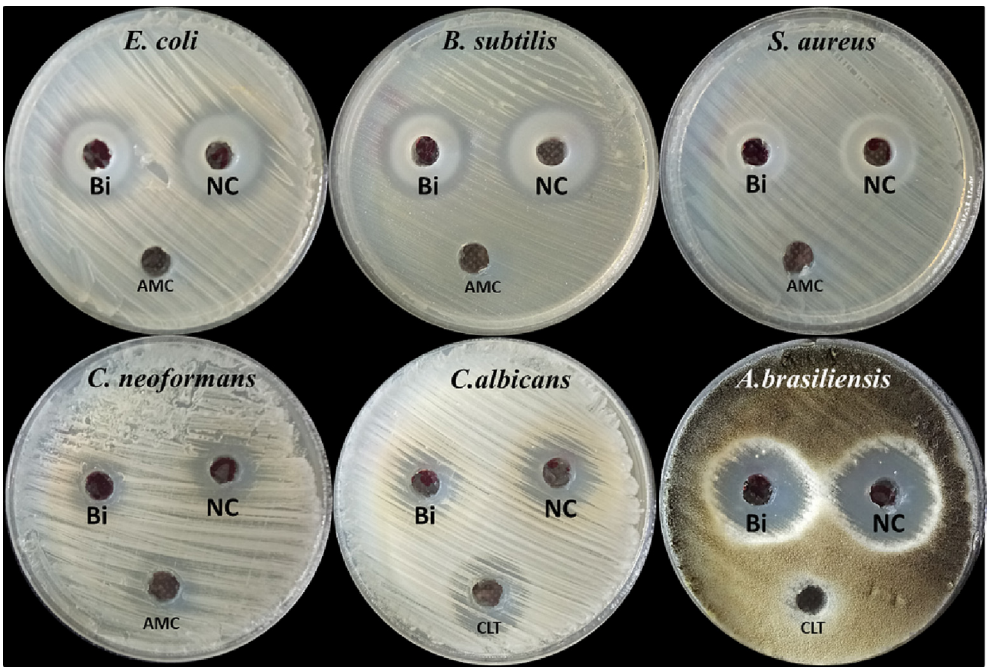

Fig. 3. Antimicrobial activity of ZnO-CuO NPs and ZnO-CuO NPs/CSC (NC) against tested bacterial and fungal strains.

Table 1
Inhibition zones and MICs of ZnO-CuO NPs and ZnO-CuO NPs/CSC against tested bacterial and fungal strains.

Test microorganism	ZnO-CuO NPs		ZnO-CuO NPs/CSC		AMC/CLT	
	IZ*	MIC μg mL^{-1}	IZ	MIC μg mL^{-1}	IZ	MIC μg mL^{-1}
E. coli	19	125	23	31.25	ND**	ND
B. subtilis	23	31.25	28	7.81	ND	ND
S. aureus	16	125	20	62.5	ND	ND
C. albicans	11	500	15	250	10	1000
C. neoformans	12	1000	17	250	10	1000
A. brasiliensis	25	15.62	28	7.81	9	1000

*IZ mean inhibition zone, **ND means no activity detected.

of protonation of the sorbent is influenced by the pH of the solution, a crucial environmental factor that also has a big impact on OH radical production, which in turn affects the specific charge of the binding sites and the sorbent's absorption capacity [67,68]. An anionic dye with a negatively charged group is called RR 195. The dye removal efficiency was greater than neutral and hence more playable at a pH value of 4.0. By elevating pH levels above 4, the removal rate was reduced [69]. The electrostatic interaction between the positively charged molecules of the biosynthesized nanocomposite and the negatively charged molecules of the dye may be the cause of the increased adsorption capacity at lower pH levels. Therefore, compared to an alkaline situation, the removal procedure was significantly more successful in an acidic condition [11,70]. On the other hand, the new strain *Shewanella xiamenensis* G5-03 has been shown by Cossolin et al. [71] to most effectively degrade the textile azo dye Reactive Red 239 between pH 8.0 and 9.0. Fig. 4 demonstrates that when catalyst concentrations rise, the initial rate improves until it reaches its maximum value and then slightly decreases at a higher concentration. Under the predetermined testing conditions, 3 μg mL^{-1} was the optimal concentration of the nanocomposite for the greatest efficiency of RR 195 degradation. In research conducted by Safari et al. [72], the rate of tetracycline degradation rose with increasing TiO_2 density and was somewhat reduced at extremely high TiO_2 concentrations under UV irradiation. By increasing the catalyst concentration, the quantity of dye molecules that were adsorbed and absorbed increased, speeding up the pace of degradation. When the catalyst concentration was boosted, elevated active sites on the photocatalyst surface produced increasing numbers of hydroxyl and superoxide radicals [73]. Furthermore, when the temperature increases, the dye adsorption decreases as the adsorption forces weaken and the connection between the adsorbent and the adsorbate decreases [74]. On the other hand, when the temperature increases, dye solubility and dissociation increase, and the contact between the adsorbate and the adsorbent reduces [29].

3.5. Reusability of ZnO-CuO-NPs/CSC nanocomposite as catalyst

Recycling tests were carried out under ideal conditions to check the stability of the ZnO-CuO-NPs/CSC photocatalyst. To do this, at the end of the fourth cycle, the photocatalyst particles were separated using centrifugation and washed with the correct proportion of ethanol to water. To create a powdered ZnO-CuO-NPs/CSC nanocomposite, the particles were oven-dried. Even after the 4th cycle of reusability, the dye removal percentage using ZnO-CuO-NPs/CSC nanocomposite showed the removal of 82.1 ± 0.41% (Fig. 5). The reason for the observed modest decrease in dye removal might be due to the buildup of organic intermediates which decreases its activity by increasing organic pollutant adsorption [75]. These outcomes were unmistakably suggestive

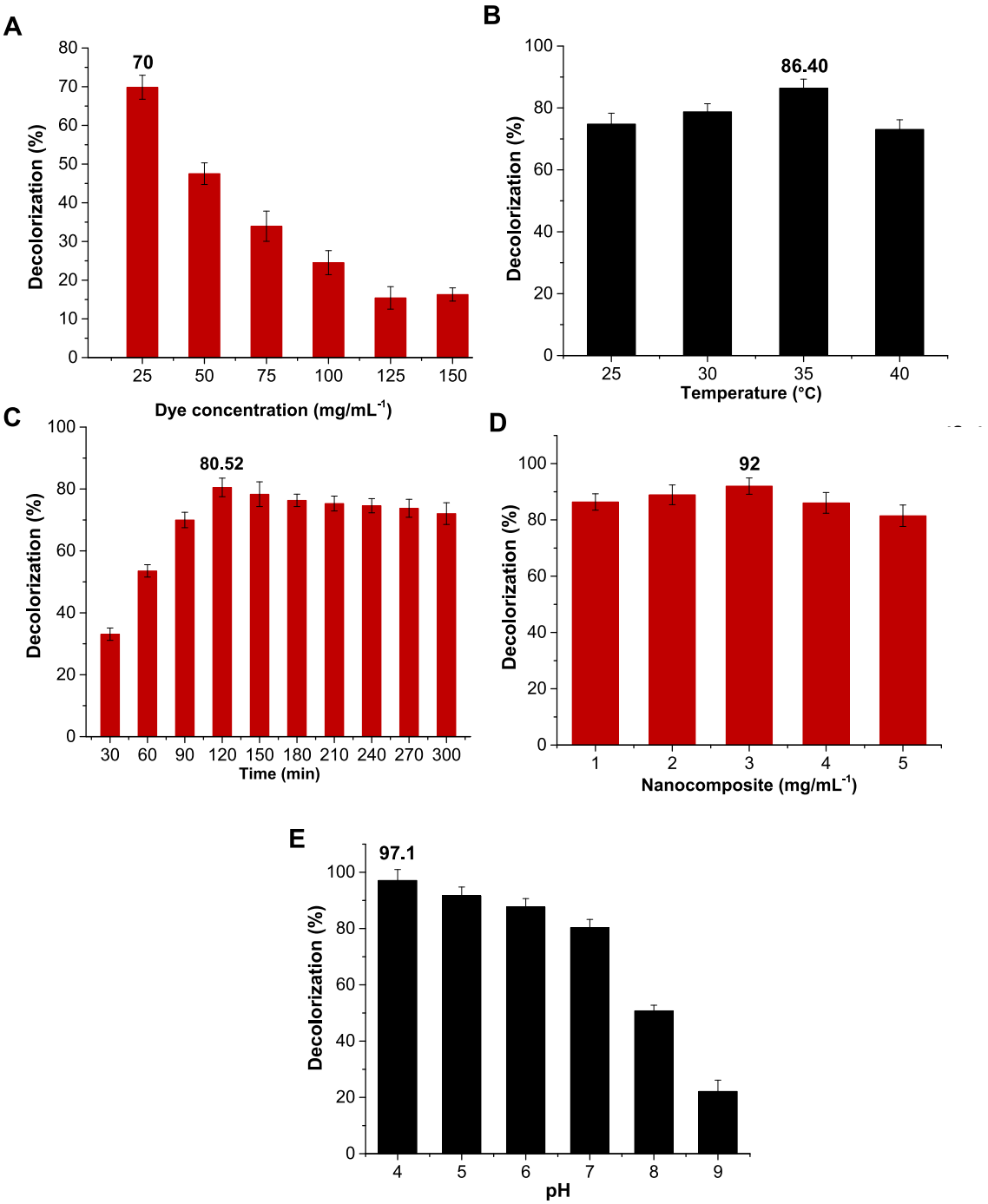

Fig. 4. **(A)** Decolourization percentages of Reactive Red 195 (RR195) dye under sunlight conditions by using 100 μg mL^{-1} of biosynthesized nanocomposite; **(B)** Study of optimizing factors for decolorizing of Reactive Red 195 (RR195) dye; **(C)** at different time intervals; different incubation temperatures (°C); **(D)** different concentrations of ZnO-CuO-NPs/CSC μg mL^{-1}; **(E)** different pH values.

of the photocatalyst's durability together with reuse for several cycles of environmentally acceptable treatments without losing its initial activity in the relevant sectors. Malekkiani et al. [30] reported that after 20 min, the MB dye's decolorization rate dropped from 98.76% at the beginning to 85% in the fourth cycle.

4. Conclusions

In the current study, a novel nanocomposite based on mycosynthesized bimetallic zinc-copper oxides nanoparticles, nanocellulose, and chitosan was prepared. Characterization of the bimetallic and nanocomposite materials was obviously performed as a nanostructure. The bimetallic materials performed particle size of less than 50 nm as well as the nanocomposite materials performed as a nanostructure. Furthermore, the nanocomposite exhibited antibacterial activity against both Gram-positive and Gram-negative bacteria. Also, it had promising antifungal activity toward unicellular and multicellular fungi. Moreover, the photocatalytic activity of a prepared nanocomposite for the decolorization of (RR195) dye has assessed and additionally, the different optimizing factors for the decolorizing have been studied.

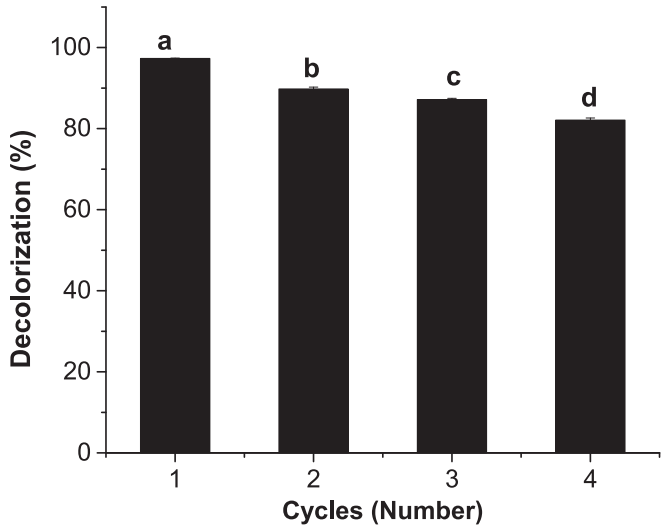

Fig. 5. ZnO-CuO-NPs/CSC nanocomposite recycling in RR195 dye removal process. Superscript letters from a to c reveal the power of significance.

Therefore, the decolorization percentage of RR195 dye was reached to 97% at 32°C, pH 4.0 and 3 μg mL^{-1} of ZnO-CuO NPs/CSC of incubation 120 min under sunlight condition. Finally, the prepared nanocomposite in this study which has antimicrobial and photocatalytic activities can be used in medical and environmental applications.

Author contributions

- Study conception and design: MS Hasanin, AH Hashem, E Saied
- Data collection: MS Hasanin, AH Hashem, AA Al-Askar, J Haponiuk, E Saied
- Analysis and interpretation of results: MS Hasanin, AH Hashem, AA Al-Askar, J Haponiuk, E Saied
- Draft manuscript preparation: MS Hasanin, AH Hashem, E Saied
- Revision of the results and approved the final version of the manuscript: MS Hasanin, AH Hashem, AA Al-Askar, J Haponiuk, E Saied

Financial support

The authors extend their appreciation to the researcher supporting project number (RSP2023R505), King Saud University, Riyadh, Saudi Arabia for funding this work.

Conflict of interest

The authors declare no conflict of interest.

Acknowledgments

The authors express their sincere thanks to the Faculty of Science (Boys), Al-Azhar University, Cairo, Egypt for providing the necessary research facilities. Also, the authors express their thanks to National Research Centre, Dokki, Egypt. Moreover, the authors extend their appreciation to the researcher supporting project number (RSP2023R505), King Saud University, Riyadh, Saudi Arabia for funding this work.

Data availability

The datasets generated during and/or analyzed during the current study are available from the corresponding authors on reasonable request.

References

[1] Al-Tohamy R, Ali SS, Li F, et al. A critical review on the treatment of dye-containing wastewater: ecotoxicological and health concerns of textile dyes and possible remediation approaches for environmental safety. Ecotoxicol Environ Saf 2022;231:. https://doi.org/10.1016/j.ecoenv.2021.113160. PMid: 35026583113160.

[2] Li F, Dong Y, Kang W, et al. Enhanced removal of azo dye using modified PAN nanofibrous membrane Fe complexes with adsorption/visible-driven photocatalysis bifunctional roles. Appl Surf Sci 2017;404:206–15. https://doi.org/10.1016/j.apsusc.2017.01.268.

[3] Pariente M, Segura Y, Molina R. Wastewater treatment as a process and a resource. In: Olivares JA, Puyol D, Melero JA, editors. Wastewater Treatment Residues as Resources for Biorefinery Products and Biofuels. Elsevier; 2020. p. 19–45. , https://doi.org/10.1016/B978-0-12-816204-0.00002-3.

[4] Kamali M, Persson KM, Costa ME, et al. Sustainability criteria for assessing nanotechnology applicability in industrial wastewater treatment: Current status and future outlook. Environ Int 2019;125:261–76. https://doi.org/10.1016/j.envint.2019.01.055. PMid: 30731376.

[5] Kokila G, Mallikarjunaswamy C, Lakshmi RV. A review on synthesis and applications of versatile nanomaterials. Inorganic Nano-Metal Chem 2022:1–30. https://doi.org/10.1080/24701556.2022.2081189.

[6] Akintelu SA, Folorunso AS, Folorunso FA, et al. Green synthesis of copper oxide nanoparticles for biomedical application and environmental remediation. Heliyon 2020;6(7):. https://doi.org/10.1016/j.heliyon.2020.e04508. PMid: 32715145e04508.

[7] Mabrouk M, Das DB, Salem ZA, et al. Nanomaterials for biomedical applications: production, characterisations, recent trends and difficulties. Molecules 2021;26(4):1077. https://doi.org/10.3390/molecules26041077. PMid: 33670668.

[8] Marouzi S, Sabouri Z, Darroudi M. Greener synthesis and medical applications of metal oxide nanoparticles. Ceram Int 2021;47(14):19632–50. https://doi.org/10.1016/j.ceramint.2021.03.301.

[9] Jeevanandam J, Kiew SF, Boakye-Ansah S, et al. Green approaches for the synthesis of metal and metal oxide nanoparticles using microbial and plant extracts. Nonoscale 2022;14(7):2534–71. https://doi.org/10.1039/D1NR08144F. PMid: 35133391.

[10] Saravanan M, Barabadi H, Vahidi H. Green nanotechnology: isolation of bioactive molecules and modified approach of biosynthesis. In: Patra C, Ahmad I, Ayaz M, editors. Biogenic Nanoparticles for Cancer Theranostics, Micro and Nano Technologies. Elsevier; 2021. p. 101–22. , https://doi.org/10.1016/B978-0-12-821467-1.00005-7.

[11] Sathiyavimal S, Vasantharaj S, Kaliannan T, et al. Eco-biocompatibility of chitosan coated biosynthesized copper oxide nanocomposite for enhanced industrial (Azo) dye removal from aqueous solution and antibacterial properties. Carbohydr Polym 2020;241:. https://doi.org/10.1016/j.carbpol.2020.116243 PMid: 32507166116243.

[12] Karagoz Y, Attar A, Arbak A, et al. Heat transfer performance of sol-gel synthesized CuONP-doped coolant in diesel engines. Case Studies in Thermal Engineering 2022;37:. https://doi.org/10.1016/j.csite.2022.102264102264.

[13] Rakhimol K, Thomas S, Kalarikkal N, et al. Casein mediated synthesis of stabilized metal/metal-oxide nanoparticles with varied surface morphology through pH alteration. Mater Chem Phys 2020;246:. https://doi.org/10.1016/j.matchemphys.2020.122803122803.

[14] Vasantharaj S, Sathiyavimal S, Saravanan M, et al. Synthesis of ecofriendly copper oxide nanoparticles for fabrication over textile fabrics: characterization of antibacterial activity and dye degradation potential. J Photochem Photobiol B Biol 2019;191:143–9. https://doi.org/10.1016/j.jphotobiol.2018.12.026. PMid: 30639996.

[15] Kumar SV, Bafana AP, Pawar P, et al. Optimized production of antibacterial copper oxide nanoparticles in a microwave-assisted synthesis reaction using response surface methodology. Colloids Surf A Physicochem Eng Asp 2019;573:170–8. https://doi.org/10.1016/j.colsurfa.2019.04.063.

[16] Gupta A, Tandon M, Kaur A. Role of metallic nanoparticles in water remediation with special emphasis on sustainable synthesis: a review. Nanotechnol Environ Eng 2020;5:27. https://doi.org/10.1007/s41204-020-00092-y.

[17] Mani VM, Kalaivani S, Sabarathinam S, et al. Copper oxide nanoparticles synthesized from an endophytic fungus *Aspergillus terreus*: Bioactivity and anti-cancer evaluations. Environ Res 2021;201:. https://doi.org/10.1016/j.envres.2021.111502. PMid: 34214561111502.

[18] Hashem AH, Khalil AMA, Reyad AM, et al. Biomedical applications of mycosynthesized selenium nanoparticles using *Penicillium expansum* ATTC 36200. Biol Trace Elem Res 2021;199:3998–4008. https://doi.org/10.1007/s12011-020-02506-z. PMid: 33387272.

[19] Salem SS, Fouda A. Green synthesis of metallic nanoparticles and their prospective biotechnological applications: an overview. Biol Trace Elem Res 2021;199:344–70. https://doi.org/10.1007/s12011-020-02138-3. PMid: 32377944.
[20] Mittal S, Roy A. Fungus and plant-mediated synthesis of metallic nanoparticles and their application in degradation of dyes. In: Shah M, Dave S, Das J, editors. Photocatalytic degradation of dyes. Elsevier; 2021. p. 287–308. PMid: 34151500 https://doi.org/10.1016/B978-0-12-823876-9.00009-3.
[21] Shaheen TI, Salem S, Fouda A. Current advances in fungal nanobiotechnology: Mycofabrication and applications. In: Lateef A, Gueguim-Kana EB, Dasgupta N, editors. Microbial Nanobiotechnology. Materials Horizons: From Nature to Nanomaterials. Singapore: Springer; 2021. p. 113–43. https://doi.org/10.1007/978-981-33-4777-9_4.
[22] Kavun V, van der Veen MA, Repo E. Selective recovery and separation of rare earth elements by organophosphorus modified MIL-101 (Cr). Microporous Mesoporous Mater 2021;312:. https://doi.org/10.1016/j.micromeso.2020.110747110747.
[23] Kumari P, Bahadur N, Dumée LF. Photo-catalytic membrane reactors for the remediation of persistent organic pollutants–a review. Sep Purif Technol 2020;230:. https://doi.org/10.1016/j.seppur.2019.115878115878.
[24] Behera M, Nayak J, Banerjee S, et al. A review on the treatment of textile industry waste effluents towards the development of efficient mitigation strategy: an integrated system design approach. J Environ Chem Eng 2021;9 (4):. https://doi.org/10.1016/j.jece.2021.105277105277.
[25] Kumawat TK, Sharma V, Kumawat V, et al. Agricultural and agro-wastes as sorbents for remediation of noxious pollutants from water and wastewater. In: Tyagi I, Goscianska J, Dehghani MH, editors. Sustainable Materials for Sensing and Remediation of Noxious Pollutants. Elsevier; 2022. p. 161–76. , https://doi.org/10.1016/B978-0-323-99425-5.00017-7.
[26] Csakvari AC, Moisa C, Radu DG, et al. Green synthesis, characterization, and antibacterial properties of silver nanoparticles obtained by using diverse varieties of *Cannabis sativa* leaf extracts. Molecules 2021;26(13):4041. https://doi.org/10.3390/molecules26134041. PMid: 34279380.
[27] Bahal M, Kaur N, Sharotri N, et al. Investigations on amphoteric chitosan/TiO_2 bionanocomposites for application in visible light induced photocatalytic degradation. Adv Polym Tech 2019;2019:2345631. https://doi.org/10.1155/2019/2345631.
[28] Joseph B, Mavelil Sam R, Balakrishnan P, et al. Extraction of nanochitin from marine resources and fabrication of polymer nanocomposites: recent advances. Polymers 2020;12(8):1664. https://doi.org/10.3390/polym12081664. PMid: 32726958.
[29] Malekkiani M, Heshmati Jannat Magham A, Ravari F, et al. Facile fabrication of ternary MWCNTs/ZnO/Chitosan nanocomposite for enhanced photocatalytic degradation of methylene blue and antibacterial activity. Sci Rep 2022;12:5927. https://doi.org/10.1038/s41598-022-09571-5. PMid: 35396520.
[30] Shaheen TI, Fouda A, Salem SS. Integration of cotton fabrics with biosynthesized CuO nanoparticles for bactericidal activity in the terms of their cytotoxicity assessment. Ind Eng Chem Res 2021;60(4):1553–63. https://doi.org/10.1021/acs.iecr.0c04880.
[31] Hasanin M, El-Henawy A, Eisa WH, et al. Nano-amino acid cellulose derivatives: Eco-synthesis, characterization, and antimicrobial properties. Int J Biol Macromol 2019;132:963–9. https://doi.org/10.1016/j.ijbiomac.2019.04.024.
[32] NCCLS. Reference Method for Broth Dilution Antifungal Susceptibility Testing of Yeasts; Approved Standard—Second Edition. NCCLS document M27-A2 (ISBN 1-56238-469-4). NCCLS, 940 West Valley Road, Suite 1400, Wayne, Pennsylvania 19087-1898 USA, 2002.
[33] Pérez-Calderón J, Santos MV, Zaritzky N. Synthesis, characterization and application of cross-linked chitosan/oxalic acid hydrogels to improve azo dye (Reactive Red 195) adsorption. React Funct Polym 2020;155:. https://doi.org/10.1016/j.reactfunctpolym.2020.104699104699.
[34] Pérez-Calderón J, Santos MV, Zaritzky N. Reactive RED 195 dye removal using chitosan coacervated particles as bio-sorbent: Analysis of kinetics, equilibrium and adsorption mechanisms. J Environ Chem Eng 2018;6(5):6749–60. https://doi.org/10.1016/j.jece.2018.10.039.
[35] Saied E, Eid AM, Hassan SED, et al. The catalytic activity of biosynthesized magnesium oxide nanoparticles (MgO-NPs) for inhibiting the growth of pathogenic microbes, tanning effluent treatment, and chromium ion removal. Catalysts 2021;11(7):821. https://doi.org/10.3390/catal11070821.
[36] Hasanin M, Swielam EM, Atwa NA, et al. Novel design of bandages using cotton pads, doped with chitosan, glycogen and ZnO nanoparticles, having enhanced antimicrobial and wounds healing effects. Int J Biol Macromol 2022;197:121–30. https://doi.org/10.1016/j.ijbiomac.2021.12.106.
[37] Barabadi H, Vahidi H, Mahjoub MA, et al. Emerging antineoplastic gold nanomaterials for cervical cancer therapeutics: A systematic review. J Clust Sci 2020;31:1173–84. https://doi.org/10.1007/s10876-019-01733-2.
[38] Mostafavi E, Zarepour A, Barabadi H, et al. Antineoplastic activity of biogenic silver and gold nanoparticles to combat leukemia: Beginning a new era in cancer theragnostic. Biotechnol Rep 2022;34:. https://doi.org/10.1016/j.btre.2022.e00714. PMid: 35686001e00714.
[39] Virmani I, Sasi C, Priyadarshini E, et al. Comparative anticancer potential of biologically and chemically synthesized gold nanoparticles. J Clust Sci 2020;31:867–76. https://doi.org/10.1007/s10876-019-01695-5.
[40] Ghareib M, Abdallah W, Abu Tahon M, et al. Biosynthesis of copper oxide nanoparticles using the preformed biomass of aspergillus fumigatus and their antibacterial and photocatalytic activities. Dig J Nanomater Biostruct 2019;14 (2):291–303.
[41] Bukhari SI, Hamed MM, Al-Agamy MH, et al. Biosynthesis of copper oxide nanoparticles using *Streptomyces* MHM38 and its biological applications. J Nanomater 2021;2021:. https://doi.org/10.1155/2021/6693302 6693302.
[42] Kumar RV, Vinoth S, Baskar V, et al. Synthesis of zinc oxide nanoparticles mediated by *Dictyota dichotoma* endophytic fungi and its photocatalytic degradation of fast green dye and antibacterial applications. S Afr J Bot 2022;151(part B):337–44. https://doi.org/10.1016/j.sajb.2022.03.016.
[43] Awan SS, Khan RT, Mehmood A, et al. *Ailanthus altissima* leaf extract mediated green production of zinc oxide (ZnO) nanoparticles for antibacterial and antioxidant activity. Saudi J Biol Sci 2023;30(1):. https://doi.org/10.1016/j.sjbs.2022.103487. PMid: 36387031103487.
[44] Kyene MO, Droepenu EK, Ayertey F, et al. Synthesis and characterization of ZnO nanomaterial from *Cassia sieberiana* and determination of its anti-inflammatory, antioxidant and antimicrobial activities. Sci Afr 2023;19:. https://doi.org/10.1016/j.sciaf.2022.e01452e01452.
[45] Fouda A, Hassan SED, Saied E, et al. An eco-friendly approach to textile and tannery wastewater treatment using maghemite nanoparticles (γ-Fe_2O_3-NPs) fabricated by *Penicillium expansum* strain (K-w). J Environ Chem Eng 2021;9 (1):. https://doi.org/10.1016/j.jece.2020.104693104693.
[46] Hunge Y, Yadav A, Kang SW, et al. Facile synthesis of multitasking composite of Silver nanoparticle with Zinc oxide for 4-nitrophenol reduction, photocatalytic hydrogen production, and 4-chlorophenol degradation. J Alloy Compd 2022;928:. https://doi.org/10.1016/j.jallcom.2022.167133167133.
[47] Albalawi MA, Abdelaziz AM, Attia MS, et al. Mycosynthesis of silica nanoparticles using *Aspergillus niger*: Control of *Alternaria solani* causing early blight disease, induction of innate immunity and reducing of oxidative stress in eggplant. Antioxidants 2022;11(12):2323. https://doi.org/10.3390/antiox11122323. PMid: 36552531.
[48] Ang W, Li X, Li S, et al. CuO nanoparticle modified ZnO nanorods with improved photocatalytic activity. Chin Phys Lett 2013;30:. https://doi.org/10.1088/0256-307X/30/4/046202046202.
[49] Truong TT, Pham TT, Truong TTT, et al. Synthesis, characterization of novel ZnO/CuO nanoparticles, and the applications in photocatalytic performance for rhodamine B dye degradation. Environ Sci Pollut Res 2022;29:22576–88. https://doi.org/10.1007/s11356-021-17106-0. PMid: 34792775.
[50] Fouda A, Salem SS, Wassel AR, et al. Optimization of green biosynthesized visible light active CuO/ZnO nano-photocatalysts for the degradation of organic methylene blue dye. Heliyon 2020;6(9):. https://doi.org/10.1016/j.heliyon.2020.e04896. PMid: 32995606e04896.
[51] Peighambardoust SJ, Peighambardoust SH, Pournasir N, et al. Properties of active starch-based films incorporating a combination of Ag, ZnO and CuO nanoparticles for potential use in food packaging applications. Food Packag Shelf Life 2019;22:. https://doi.org/10.1016/j.fpsl.2019.100420100420.
[52] Xu L, Su J, Zheng G, et al. Enhanced photocatalytic performance of porous ZnO thin films by CuO nanoparticles surface modification. Mater Sci Eng B 2019;248:. https://doi.org/10.1016/j.mseb.2019.114405114405.
[53] Hasanin MS, Youssef AM. Ecofriendly bioactive film doped CuO nanoparticles based biopolymers and reinforced by enzymatically modified nanocellulose fibers for active packaging applications. Food Packag Shelf Life 2022;34:. https://doi.org/10.1016/j.fpsl.2022.100979100979.
[54] Hashem AH, Al Abboud MA, Alawlaqi MM, et al. Synthesis of nanocapsules based on biosynthesized nickel nanoparticles and potato starch: Antimicrobial, antioxidant and anticancer activity. Starch-Stärke 2021;74(1–2):2100165. https://doi.org/10.1002/star.202100165.
[55] Iashin I, Hasanin M, Hassan SAM, et al. Green biosynthesis of zinc and selenium oxide nanoparticles using callus extract of *Ziziphus spina-christi*: Characterization, antimicrobial, and antioxidant activity. Biomass Convers Biorefin 2021. https://doi.org/10.1007/s13399-021-01873-4.
[56] Ibrahim S, Elsayed H, Hasanin M. Biodegradable, antimicrobial and antioxidant biofilm for active packaging based on extracted gelatin and lignocelluloses biowastes. J Polym Environ 2021;29:472–82. https://doi.org/10.1007/s10924-020-01893-7.
[57] Shehabeldine A, El-Hamshary H, Hasanin M, et al. Enhancing the antifungal activity of griseofulvin by incorporation a green biopolymer-based nanocomposite. Polymers 2021;13(14):542. https://doi.org/10.3390/polym13040542.
[58] Shukla P, Tiwari S, Joshi SR, et al. Investigation on structural, morphological and optical properties of Co-doped ZnO thin films. Physica B: Condensed Matter 2018;550:303–10. https://doi.org/10.1016/j.physb.2018.08.046.
[59] Mariammal RN, Ramachandran K. Study on gas sensing mechanism in p-CuO/n-ZnO heterojunction sensor. Mater Res Bull 2018;100:420–8. https://doi.org/10.1016/j.materresbull.2017.12.046.
[60] Nagarani S, Sasikala G, Yuvaraj M, et al. ZnO-CuO nanoparticles enameled on reduced graphene nanosheets as electrode materials for supercapacitors applications. J Storage Mater 2022;52(part C):104969. https://doi.org/10.1016/j.est.2022.104969.
[61] Abdelraof M, Ibrahim S, Selim MH, et al. Immobilization of L-methionine γ-lyase on different cellulosic materials and its potential application in green-selective synthesis of volatile sulfur compounds. J Environ Chem Eng 2020;8 (4):. https://doi.org/10.1016/j.jece.2020.103870103870.

[62] Turky G, Moussa MA, Hasanin M, et al. Carboxymethyl cellulose-based hydrogel: dielectric study, antimicrobial activity and biocompatibility. Arab J Sci Eng 2021;46:17–30. https://doi.org/10.1007/s13369-020-04655-8.
[63] Baptista PV, McCusker MP, Carvalho A, et al. Nano-strategies to fight multidrug resistant bacteria—"A Battle of the Titans". Front Microbiol 2018;9:1441. https://doi.org/10.3389/fmicb.2018.01441. PMid: 30013539.
[64] Arora N, Thangavelu K, Karanikolos GN. Bimetallic nanoparticles for antimicrobial applications. Front Chem 2020;8:412. https://doi.org/10.3389/fchem.2020.00412. PMid: 32671014.
[65] Truong LB, Medina-Cruz D, Martínez-Sanmiguel JJ, et al. Biogenic metal nanomaterials to combat antimicrobial resistance. In: Saravanan M, Barabadi H, Mostafavi E, editors. Micro and Nano Technologies, Emerging Nanomaterials and Nano-Based Drug Delivery Approaches to Combat Antimicrobial Resistance. Elsevier; 2022. p. 261–304. , https://doi.org/10.1016/B978-0-323-90792-7.00011-7.
[66] Ali AA, Ahmed IS, Amin AS, et al. Auto-combustion fabrication and optical properties of zinc oxide nanoparticles for degradation of reactive red 195 and methyl orange dyes. J Inorg Organomet Polym Mater 2021;31:3780–92. https://doi.org/10.1007/s10904-021-01975-6.
[67] Bhatia M, Satish Babu R, Sonawane S, et al. Application of nanoadsorbents for removal of lead from water. Int J Environ Sci Technol 2017;14:1135–54. https://doi.org/10.1007/s13762-016-1198-6.
[68] Tang F, Yu H, Abdalkarim SYH, et al. Green acid-free hydrolysis of wasted pomelo peel to produce carboxylated cellulose nanofibers with super absorption/flocculation ability for environmental remediation materials. Chem Eng J 2020;395:. https://doi.org/10.1016/j.cej.2020.125070125070.
[69] Munagapati VS, Wen HY, Gollakota ARK. Removal of sulfonated azo Reactive Red 195 textile dye from liquid phase using surface-modified lychee (Litchi chinensis) peels with quaternary ammonium groups: Adsorption performance, regeneration, and mechanism. J Mol Liq 2022;368(Part A). https://doi.org/10.1016/j.molliq.2022.120657.
[70] Aghajari N, Ghasemi Z, Younesi H, et al. Synthesis, characterization and photocatalytic application of Ag-doped Fe-ZSM-5@ TiO_2 nanocomposite for degradation of reactive red 195 (RR 195) in aqueous environment under sunlight irradiation. J Environ Health Sci Eng 2019;17:219–32. https://doi.org/10.1007/s40201-019-00342-5 PMid: 31321045.
[71] Cossolin AS, Reis HCO, Castro KC, et al. Decolorization of textile azo dye Reactive Red 239 by the novel strain *Shewanella xiamenensis* G5–03 isolated from contaminated soil. Rev Ambiente Água 2019;14(6):e2446.
[72] Safari G, Hoseini M, Seyedsalehi M, et al. Photocatalytic degradation of tetracycline using nanosized titanium dioxide in aqueous solution. Int J Environ Sci Technol 2015;12:603–16. https://doi.org/10.1007/s13762-014-0706-9.
[73] Rafiq A, Ikram M, Ali S, et al. Photocatalytic degradation of dyes using semiconductor photocatalysts to clean industrial water pollution. J Ind Eng Chem 2021;97:111–28. https://doi.org/10.1016/j.jiec.2021.02.017.
[74] Abd Malek NN, Jawad AH, Ismail K, et al. Fly ash modified magnetic chitosan-polyvinyl alcohol blend for reactive orange 16 dye removal: Adsorption parametric optimization. Int J Biol Macromol 2021;189:464–76. https://doi.org/10.1016/j.ijbiomac.2021.08.160 PMid: 34450144.
[75] Kucukcongar S, Alwindawi AGJ, Turkyilmaz M, et al. Reactive dye removal by photocatalysis and sonophotocatalysis processes using $Ag/TiO_2/Fe_3O_4$ nanocomposite. Water Air Soil Pollut 2023;234:103. https://doi.org/10.1007/s11270-023-06136-8.